Absorption coefficient and purine photobleaching rate in colon mucosa during resonance Raman spectroscopy at 251 nm

Nada N. Boustany

In contrast to spectroscopy at longer wavelengths, typical attributes of ultraviolet resonance Raman (UVRR) spectroscopy of biologic tissue are higher absorption coefficient, μ, and higher photobleaching rate, κ. This study was aimed at measuring μ and κ during UVRR spectroscopy of human colon tissue at 251 nm. μ was used to estimate the penetration depth of the excitation light; κ was used to predict the rate of signal decrease that was due to photobleaching as a function of laser fluence and tissue thickness. The fitting of the equations through description of a three-state transition model to experimental data that consisted of a purine UVRR signal gave $\mu = 0.0169 \pm 0.0023\ \mu m^{-1}$ and $\kappa = 0.572 \pm 0.168\ (mJ/\mu m^2)^{-1}$. κ remained independent of power P for $P < 1$ mW, but higher power values resulted in a higher photobleaching rate. As predicted by the model, signal decrease that was due to photobleaching was slower as sample thickness was increased. © 2001 Optical Society of America

OCIS codes: 300.6450, 170.5660, 170.6390, 260.5130, 260.5740, 260.7190.

1. Introduction

Optical spectroscopic techniques increasingly are being evaluated for their possible applications as probes of human disease and biologic function. Among these spectroscopic techniques ultraviolet resonance Raman (UVRR) spectroscopy is being used to study biochemical processes involving proteins, microorganisms, cells, and tissues.[1–8] In resonance Raman spectroscopy, the energy of the excitation light is tuned closely to an electronic transition of the molecule being interrogated, and vibrations coupled to the molecule's excited electronic state are enhanced preferentially. While this tuning of the excitation wavelength increases the detection sensitivity for compounds that are present in low concentrations, it also implies that during resonance Raman spectroscopy the optically interacting molecules are pumped from one energy level (usually the ground state) to an excited state, and may assume an upper molecular-electronic/vibrational state for a duration of time. Single-photon absorptions are especially prevalent, since the excitation light is tuned to molecular-absorption bands.

For the intensity of the Raman-scattered light to remain constant with time (or for the time-integrated Raman signal to increase linearly with time without saturating), the number of scattering molecules in the ground state must remain constant to provide a fixed density of interaction sites for incident photons. However, it is possible to deplete the ground-state concentration of Raman-active molecules in a process known as photobleaching. Photobleaching results in the saturation of the time-integrated Raman signal and can occur when the rate at which the molecules return to the original ground state is slower than the rate of optical pumping, or when the excited molecules are chemically altered to species that do not have the same emission properties as the original molecules. In the first case, photobleaching is reversible as the Raman-active molecules return to their original ground state. In the second case, photobleaching is irreversible, and the molecules are permanently altered. In our studies we observed irreversible purine photobleaching. As will be shown, photobleaching depends on a tissue's optical properties, such as its light-absorption coefficient,

When this research was performed, the author (boustany@bme.jhu.edu) was with the George R. Harrisson Spectroscopy Laboratory, Massachusetts Institute of Technology, and the Harvard-MIT Division of Health Sciences and Technology, Cambridge, Massachusetts 02139. He is currently with the Biomedical Engineering Department, Johns Hopkins University School of Medicine, 720 Rutland Avenue, Traylor 701, Baltimore, Maryland 21205.

Received 1 May 2001; revised manuscript received 23 July 2001.
0003-6935/02/346396-10$15.00/0

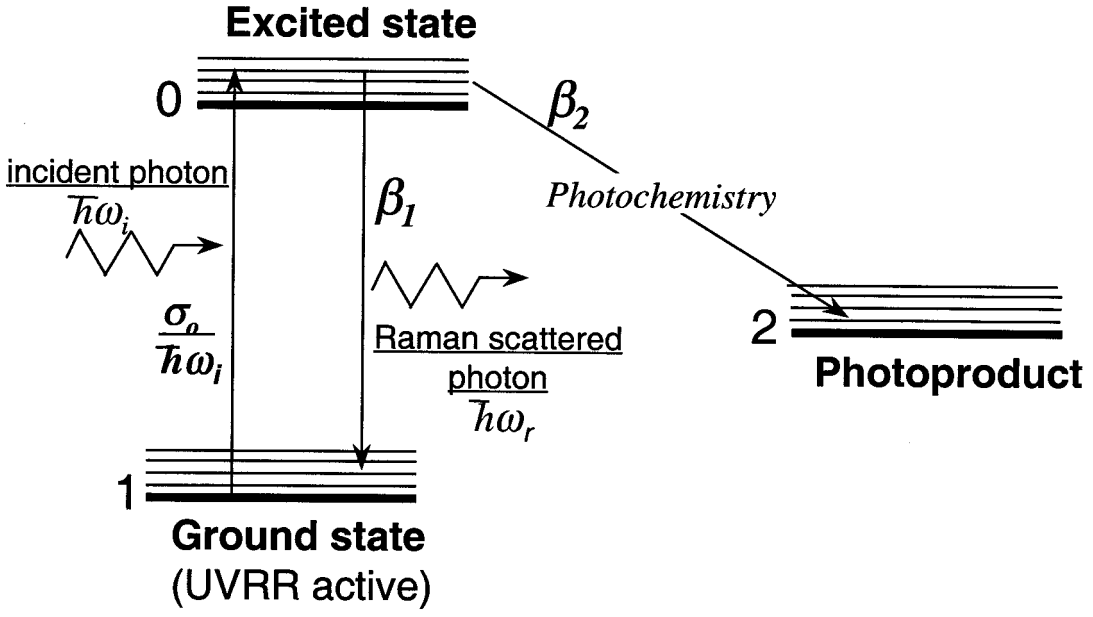

Fig. 1. Energy diagram showing the transitions of a model Raman-active species undergoing photochemistry. The ground-state Raman-active species is pumped to an excited state by absorption of an incident photon of energy $\bar{h}\omega_i$. The absorption coefficient is σ_0. β_1 and β_2 represent the transition rates at which the excited species returns to the ground state and undergoes photochemistry, respectively. If the molecule returns to the ground state, the incident photon is scattered as a Raman photon with energy $\bar{h}\omega_r$. The overall transition probability κ from the ground state to the photoproduct state is given by Eq. (1).

and the transition rate of the Raman-active molecules between the ground state and the photobleached state.

In this paper a physical evaluation of the photobleaching process in human colon mucosa is presented. To describe purine photobleaching, a three-state transition model is developed, and its predictions are compared with experimental results that were obtained by monitoring the purine UVRR band in the colon spectra. The rate of purine photobleaching as a function of excitation light fluence and tissue thickness is described. The light attenuation coefficient and the optical penetration depth of 251-nm light in colon mucosa are also measured. The values of the absorption coefficient μ and the photobleaching rate κ measured in this study can be used to improve experimental design and data interpretation during future UVRR spectroscopy of biologic tissue.

2. Physical Model of Photobleaching

In this section, a physical model is developed to describe purine photobleaching in colon UVRR spectra. We assume that the photobleaching of colon tissue is due to photoreactive molecules that form new species during UV irradiation and not due to long-lived molecular excited states, since the photobleaching was experimentally found to be irreversible. Figure 1 illustrates a possible transition between a molecule's ground state (state 1) and the photoproduct state (state 2). The probability of transition per unit energy dose (κ) between these states can be written as

$$\kappa = \frac{\sigma_0}{\bar{h}\omega_i}\left(\frac{\beta_2}{\beta_1 + \beta_2}\right), \qquad (1)$$

where σ_0 is the absorption cross section for a transition between the ground state and the first excited state, and $\bar{h}\sigma_i$ is the energy of the incident photon. β_1 and β_2 are the decay rates between the excited state and the ground state and between the excited and the photodegraded state, respectively. The branching ratio, $\beta_2/(\beta_1 + \beta_2)$, determines the probability of photoproduct generation. If the molecule returns to the ground state, the incident photon is scattered as a Raman photon with energy $\bar{h}\sigma_r$.

The tissue is assumed to be homogeneous and contain a density of n_a absorbers and n_r Raman scatterers per unit volume. The resonance Raman-scattering signal considered in this study is generated by n_r, the density of purines in the tissue. The quantity of these species may decrease, owing to the formation of nonscattering photoproducts. However, purine photoproducts still absorb at 250 nm.[9] Moreover, other tissue constituents, such as proteins, which exist in much higher concentrations than nucleic acids, may also continue to absorb at 250 nm. Thus we assume that $n_a \sim$ constant, while n_r will decrease, owing to photoproduct formation.

This physical system can be studied in the simple case of a collimated optical beam propagating through tissue of thickness Z_0 and where Raman scattering from Raman-active molecules is collected in a backreflection geometry (Fig. 2). Even though experimentally the sample is irradiated by a focused laser beam, we assume that the penetration depth of the light in the tissue is shorter than the lens's Rayleigh range, which was 80 μm.

The decrease of n_r as a function of time t is assumed to be linear with laser intensity, transition rate κ, and

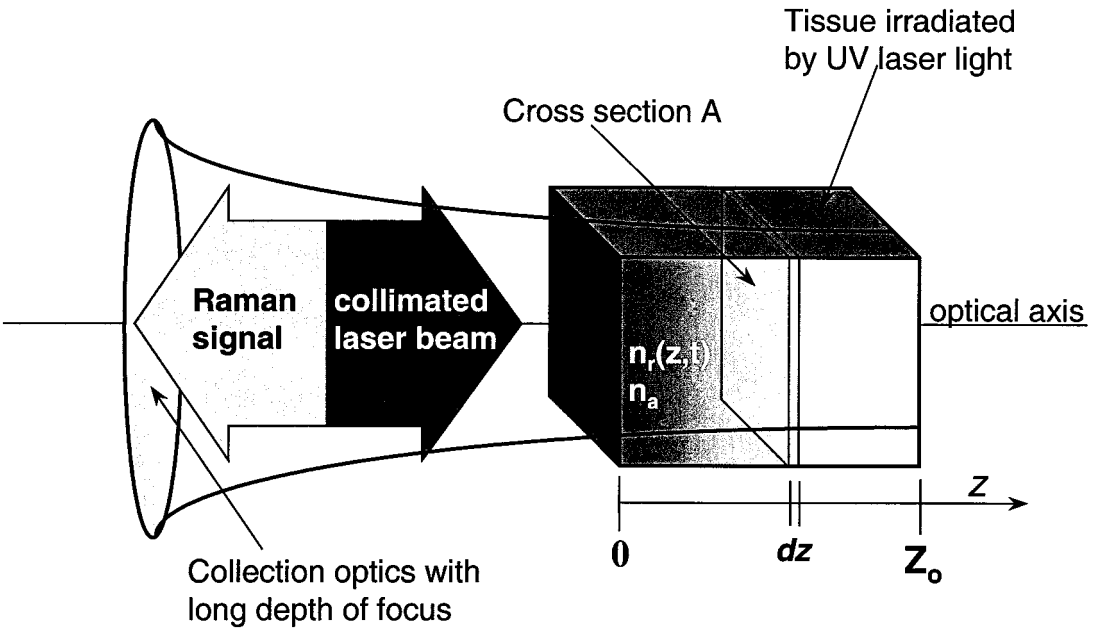

Fig. 2. Schematic of a model Raman-scattering tissue sample irradiated by a collimated laser beam. The tissue of thickness Z_0 and cross section A is assumed to be homogeneous with a uniform initial density of Raman scatterers n_{ro} and a uniform density of absorbers n_a. While the number of Raman scatterers decreases as photobleaching progresses, the density of absorbers in the tissue is assumed to remain constant. The Raman-scattering signal is collected in a 180° backscattering geometry. The large f/# of the excitation/collection lens ensures that the intensity of the excitation light is constant within a given cross section and that the Raman signal is collected equally from all cross sections.

n_r. The change in intensity I as a function of distance into the tissue z is described by Beer's law with attenuation coefficient μ. Assuming that attenuation that is due to elastic scattering is much smaller than that which is due to absorption, the attenuation coefficient μ could be written as $\mu \sim \sigma_0 n_a$, and the two processes can be described as

$$\frac{\partial n_r}{\partial t} = -\kappa I n_r, \tag{2}$$

$$\frac{\mathrm{d}I}{\mathrm{d}z} = -\mu I. \tag{3}$$

We assumed that the number of absorbers n_a remains constant. Thus the light intensity I is a function of only z, and the equations are decoupled. Equations (2) and (3) simplify to

$$I(z) = I_0 \exp(-\mu z), \tag{4}$$

$$n_r(t, z) = n_{ro} \exp(-\kappa I t) = n_{ro} \exp[-\kappa I_0 \exp(-\mu z) t], \tag{5}$$

where I_0 is the excitation light intensity at the surface of the tissue ($z = 0$) and n_{ro} is the initial density of Raman scatterers $n_r(t = 0)$.

The Raman signal as a function of time, $S_R(t)$, can be written as

$$S_R(t) = \sigma_r A \int_0^{Z_0} K(z) n_r(t, z) I(z) \exp(-\mu z) \mathrm{d}z, \tag{6}$$

where σ_r is the Raman-scattering cross section per molecule, A is the cross-section area of the examined tissue volume (see Fig. 2), and K is the collection efficiency of the system. Strictly speaking, K is a function of the distance into the tissue, since light scattered from molecules located deeper in the tissue will be collected with a smaller solid angle compared with that scattered from molecules closer to the tissue surface. However, since the focal length of the collection system is larger than the excited-tissue depth ($1/\mu$), this collection efficiency is assumed to be a constant over the length of the tissue sample, i.e., $K(z) = K_0$. The exponential factor inside the integral represents the attenuation of the Raman-scattered light as it travels from the scattering center to the surface of the tissue. Since the wavelength of the Raman-scattered light is within ~10 nm of the excitation wavelength, the tissue attenuation coefficient μ is assumed to be the same for both the excitation and the scattered light.

By letting $u = \exp(-\mu z)$, the integral in Eq. (6) can be solved as

$$\begin{aligned} S_R(t) &= \sigma_r K_0 A \int_1^{\exp(-\mu Z_0)} n_r I_0 u^2 \frac{\mathrm{d}u}{-\mu u} \\ &= \sigma_r K_0 A\, n_{ro} \frac{I_0}{\mu} \int_1^{\exp(-\mu Z_0)} -u \exp(-\kappa I_0 t u) \mathrm{d}u \\ &= \frac{C_R}{\mu} \int_1^{\exp(-\mu Z_0)} -u \exp(-\kappa \Phi u) \mathrm{d}u, \end{aligned} \tag{7}$$

where the fluence $\Phi = I_0 t$ is the energy dose delivered to the tissue and the constant $C_r \equiv K_0 A I_0 \sigma_r n_{ro}$ accounts for the laser intensity, the light delivery and collection geometry, the Raman cross section, and the initial density of scatterers in the tissue. The solving of this integral reduces Eq. (7) to

$$S_R(\Phi) = \frac{C_R}{\mu(\kappa\Phi)^2}\{\exp[-\kappa\Phi\exp(-\mu Z_0)] \times [\kappa\Phi\exp(-\mu Z_0) + 1] - \exp(-\kappa\Phi)(\kappa\Phi + 1)\}, \quad (8)$$

which is the desired expression for the measured Raman signal as a function of fluence for a given thickness of tissue Z_0.

As will be found, the bands in colon spectra that photobleach do not completely decay as predicted by Eq. (8). Instead, they decrease to an asymptotic value. This residual signal can be accounted for by altering Eq. (5) and adding a density of n_{res} nonphotobleaching molecules, with Raman cross section σ_{res}, to give a total density of Raman scatterers n_T:

$$n_T = n_{ro}\exp(-\kappa I t) + n_{res}. \quad (9)$$

This gives a total Raman signal $S_T(\Phi)$,

$$S_T(\Phi) = S_R(\Phi) + \frac{C_{res}}{2\mu}[1 - \exp(2\mu Z_0)] \equiv S_R(\Phi) + S_{res}, \quad (10)$$

where $C_{res} \equiv K_0 A I_0 \sigma_{res} n_{res}$. The nonphotobleaching residual molecules n_{res} may have Raman-scattering properties different from those of the photobleaching Raman species that are represented by n_{ro}. Thus in general σ_{res} is assumed to be different from σ_r.

Limiting cases of Eq. (10) are important to consider, since they will be used to determine the values of some of the constants governing photobleaching. For small values of Φ ($\kappa\Phi \ll 1$):

$$S_T(\Phi \sim 0) = S_R(\Phi \sim 0) + S_{res} = \left(\frac{C_R + C_{res}}{2\mu}\right) \times [1 - \exp(-2\mu Z_0)]. \quad (11)$$

For the signal strength after a large fluence was delivered to the tissue,

$$S_T(\Phi \to \infty) = S_{res}. \quad (12)$$

For very thin sections with $Z_0 \ll 1/\mu$, the intensity I is approximately constant over the thickness of the tissue [$I(z) \sim I_0$]. In this case the signal is only a function of fluence, and

$$S_T(\Phi)|_{Z_0 \to 0} \approx C_R Z_0 \exp(-\kappa\Phi) + C_{res} Z_0. \quad (13)$$

For very thick sections with $Z_0 \gg 1/\mu$,

$$S_T(\Phi)|_{Z_0 \to \infty} \approx \frac{C_R}{\mu(\kappa\Phi)^2}[1 - \exp(-\kappa\Phi) \times (\kappa\Phi + 1)] + \frac{C_{res}}{2\mu}. \quad (14)$$

3. Materials and Methods

A. Ultraviolet Resonance Raman Spectroscopy Instrumentation and Sample Preparation

The UVRR microscopy system, which was used to collect the spectra, was described previously in detail.[8] The excitation source uses the third harmonic of a tunable, argon-laser-pumped, mode-locked Ti: sapphire laser (Coherent, Inc.). The laser- excitation wavelength was tuned to 251 nm. This quasi-continuous laser system produces 2–3-ps pulses at 76 MHz. The collected Raman-scattered light is launched into a 1-m-long f/8 spectrometer (SPEX/Jobin-Yvon) that disperses it at 0.4nm/mm with a single 2400-grooves/mm grating across a liquid-nitrogen-cooled CCD detector (Princeton Instruments). The system resolution was 15 cm^{-1}. This is adequate for Raman studies of biologic tissue, which has Raman bands ~30 cm^{-1} wide.

The UV excitation light was shaped by two lenses, redirected with a beam splitter, and focused onto the sample with a Cassegrain microscope objective. Scattered light was collected by the same objective, through the beam splitter, and then directed and focused on the spectrometer entrance slit. A neutral density filter was placed in the excitation light path to control sample illumination power to 0.17–0.25mW. In one study, the effects of laser power on photobleaching were investigated by varying the excitation power between 0.2 and 3 mW. The 15× reflecting objective (Ealing Electro-optics, Holliston, Mass., Model 25-0506) used in this study yielded a spot diameter of 5 μm. The depth of field was measured as 80 μm. The microscope stage was cooled to 0–4 °C.

A dielectric longpass filter (Barr Associates, Westford, Mass.) or liquid-solution filter was placed in the light-scattering collection path to reject the Rayleigh-scattered light. The solution was prepared from a stock containing 2.5×10^{-5} M anthracene and 0.5 M KI dissolved in ethanol:water (1:1::V:V). The stock was subsequently diluted 13 times in pure ethanol and placed in a 1-cm path length quartz cuvette. The filter solution was renewed before every experimental run, and its absorption spectrum was measured and found to be consistent before and after each run and from day to day. Spectra of ethanol and acetone were collected to calibrate the Raman shift axis in the wavenumber range 1000–1800 cm^{-1}. Utilizing the known Raman band positions of ethanol and acetone,[10–11] we used a third-order polynomial interpolation to convert CCD pixel numbers to wave numbers.[12] The spectra were not intensity calibrated, since this calibration was not necessary for

these studies, where relative changes in Raman intensity are considered.

Normal human colon tissue was used in the study and was obtained after surgical resection. Briefly, partial colectomy specimens were resected from patients with colonic cancer. Within 10 min of receipt from the operating room, 1 cm × 1 cm full-thickness samples of normal colonic tissue at least 3 cm from the colon cancer were prepared by way of scalpel incision. These samples consisted of normal colonic mucosa, submucosa, muscle wall, and serosa. The collected tissue was snap frozen in liquid nitrogen and stored at −80 °C until use. Microscopic frozen sections were prepared through sectioning of the frozen tissue perpendicular to the mucosal surface with a microtome into slices between 12 and 400 μm thick. During data acquisition, the microscope stage was set so that the middle of the thickest tissue section was positioned in the waist of the focused laser beam to minimize variations in signal intensity due to the collection geometry of the instrument.

B. Raman Signal Analysis

Photobleaching was quantified through the monitoring of the intensity of the purine Raman band that was centered at 1485 cm^{-1} in the colon mucosa spectrum. The strength of the 1485 cm^{-1} band was measured as a function of laser energy and tissue-section thickness during sample irradiation. Collected spectra were fitted in the range of 1450–1550 cm^{-1} to a guanosine monophosphate line shape and a constant background by least-squares minimization (LSM). The LSM weighting parameter for guanosine monophosphate is indicative of the area under the 1485 cm^{-1} peak after background subtraction. Instead of simply integrating under the band, this LSM fitting technique was used to improve background signal subtraction. The 1485 cm^{-1} peak has contributions from adenosine as well as guanosine. However, these compounds have the same line shape between 1450 and 1550 cm^{-1}, and only one was used in the fit to determine peak areas.

The UVRR signal was recorded as a function of time through the sequential acquisition of consecutive spectra, each with a collection time of 100 s, from a given point on the mucosa. Then the excitation beam was moved, and the sequential collection repeated at other locations. For each 100-s time interval, data collected from the different point locations on the mucosa were subsequently averaged. Each 100-s time interval Δt was assumed to correspond to an instantaneous time value and therefore an instantaneous value of fluence Φ. The signal that was collected in the first time interval was taken to correspond to the initial Raman signal value for $\Phi \rightarrow 0$. The second interval corresponded to $\Phi(\Delta t)$, the third to $\Phi(2\Delta t)$, and so forth. Signal strength was plotted as a function of these fluence values and of sample thickness and compared with the photobleaching model predictions. Marquardt's method[13] was used to solve for the tissue parameters and instrumentation constants through the fitting of the nonlinear model equations (Section 2) to the data.

C. Absorption Spectrophotometry

The attenuation coefficient of colon tissue at 250 nm was measured by absorption spectrophotometry. Colon mucosa was sliced perpendicular to the crypts (parallel to the mucosal surface) into 10-150-μm thin sections. These were hydrated with ~10 μl of phosphate-buffered saline, mounted between two quartz plates, and placed into an absorption spectrophotometer (Shimatzu UV-265). The quartz windows were apertured (2 × 2 mm square) to prevent light from reaching the detector without being transmitted through the tissue. All sections (unstained) were inspected under a light microscope to verify that the tissue filled the aperture and that the tissue in the aperture was from the mucosal region. Light absorption was measured as a function of tissue thickness. A LSM was used to fit a straight line to the data. The slope of this line was used to calculate the attenuation coefficient μ.

The accuracy of the microtome thickness settings was checked by making 12- and 24-μm thin tissue sections and mounting them on the edge of a quartz plate. This plate was mounted perpendicularly on a glass slide, so that the edge of the plate and the thickness of the attached tissue could be viewed under a light microscope. Thicknesses were measured with a reticle at different points along the tissue slices.

4. Results

A. Measurement of Tissue Optical Parameters

1. Rate of Photoproduct Formation

The purine Raman signal at 1485 cm^{-1} is plotted as a function of fluence delivered to the tissue for a nominal 12-μm thin colon-tissue section (Fig. 3). As will be seen later, this section is significantly thinner than $1/\mu$ and should have a fairly uniform light intensity throughout its thickness. Thus the photobleaching may be modeled by relation (13). To determine the transition rate κ, we fitted relation (13) to the data in Fig. 3 by varying C_R, C_{res}, and κ and setting $Z_0 = 12$ μm. The result of the fit yielded the probability of transition, per unit fluence, of the scattering purines from the ground state to a photobleached state, $\kappa = 0.572 \pm 0.168\ (mJ/\mu m^2)^{-1}$, $C_R = 0.0727 \pm 0.0083$, and $C_{res} = 0.0244 \pm 0.0053$. The errors listed here were computed from the variances of the fit parameters, given the average confidence interval of the data. Thus at $\Phi = 1.75\ mJ/\mu m^2$ (= $1/\kappa$) the Raman signal from a cooled thin colon-tissue section (thickness $\ll 1/\mu$) will reach ~63% of its initial value. The laser intensity I_0 was 0.012 $mW/\mu m^2$ in this experiment. For typical values of I_0 ~0.01 $mW/\mu m^2$, $\Phi = 1.75$ is reached in 175 s.

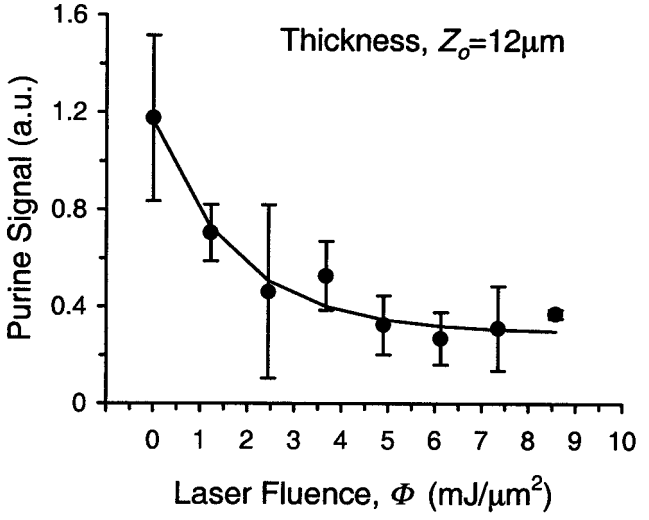

Fig. 3. Estimation of photobleaching rate κ. Purine signal data (filled circles) were plotted as a function of laser fluence Φ for the case of a 12-μm thin section [$Z_0 \ll 1/\mu$, $I(z) \sim$ constant $= I_0$]. Relation (13) was fitted to the data by a nonlinear fitting routine (solid line). The fit yielded $\kappa = 0.572 \pm 0.168$ $(\text{mJ}/\mu\text{m}^2)^{-1}$. The error bars represent the standard deviation of the mean.

2. *Light Attenuation Coefficient*

The attenuation coefficient of colon mucosa was determined through measurement of the initial signal strength (first 100-s interval of data collection, $\Phi \sim 0$) from several sections of cooled tissue of different thicknesses. Equation (11) was fitted to the data. The best fit gave an attenuation coefficient of $\mu = 0.0169 \pm 0.0023$ μm^{-1}, and $(C_R + C_{\text{res}})/2\mu = 1.73$. The error in μ was computed from the variance of the fit parameter, given the average confidence interval of the data. Figure 4A shows the signal strength of the purine band as a function of sample thickness (filled circles), and the model fit (solid curve). In this experiment, the laser intensity I_0 was 0.0086 mW/μm^2. Utilizing the present value of $\mu = 0.0169$, $C_R = 0.0727$, and $C_{\text{res}} = 0.0244$ from the fit of the previous data in Fig. 3, we can recalculate $(C_R + C_{\text{res}})/2\mu = 2.87$. In Fig. 4A, the laser intensity I_0 was 0.0086 mW/μm^2, namely, 70% of the intensity level in the thin slice experiment of Fig. 3. This will correspond to an equivalent drop in C_R and C_{res}. Thus we can correct our calculated value to $(0.7)(C_R + C_{\text{res}})/2\mu = 2.01$. This value is within 15% of 1.73, the value extracted from the present data fit (data of Fig. 4). In general C_R and C_{res} are dependent on the local concentration of scatterers in a given tissue section and on potential laser power fluctuations; thus they were kept as variables in the model fits.

The absorbance A of colon mucosa versus tissue thickness measured by spectrophotometry is plotted in Fig. 4B. A linear least-squares fit to the data gave a slope of 0.00694 ± 0.00108 μm^{-1} and an intercept of 0.22 ± 0.073. The coefficient of correlation was 0.82. The nonzero offset in the fitted line is probably caused by reflection losses at the tissue/saline interface, owing to index mismatches, which can be non-

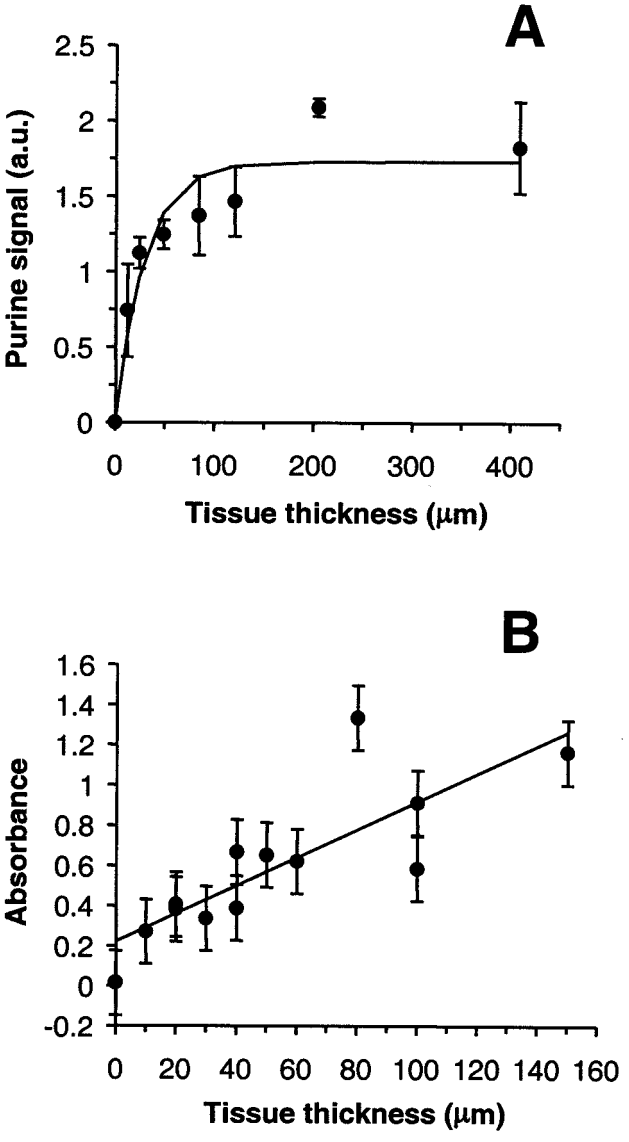

Fig. 4. Estimation of attenuation coefficient μ by purine Raman signal measurement (panel A) and by absorption spectrophotometry (panel B). A, Purine Raman signal (filled circles) measured as a function of tissue thickness (Z_0); Equation (11) ($\Phi \sim 0$) was fitted to the data by a standard nonlinear fitting routine (solid curve). The fit yielded $\mu = 0.0169 \pm 0.0023$ μm^{-1}. The error bars represent the standard deviation of the mean. B, Absorbance was measured and plotted as a function of tissue thickness. A straight line (solid line) was fitted to the data (filled circles), including the (0,0) point (no tissue present), by a least-squares-fitting routine. The fit yielded $\mu = 0.00160 \pm 0.0025$ μm^{-1}. The coefficient of correlation was 0.82. The error bar, σ_y shown on the graph, was estimated from the fit as $\sigma_y = [(1/N - 2)\Sigma i = 1/N(y_i - y_{\text{fit}})^2$ (Ref. 29).

negligible at wavelengths shorter than ~300 nm.[14] Since $A = \log(e^{\mu z})$, the slope $dA/dz = \mu \log_{1_0} e$ (after offset subtraction, with $e = 2.718$). This gives $\mu = 0.0160 \pm 0.0025$ μm^{-1}, which agrees well with the attenuation coefficient that was calculated from the Raman band-signal intensity (Fig. 4A). The penetration depth, or $1/\mu$, is therefore ~60 μm as measured by two independent methods.

When a nominal 12-μm section was obtained with the microtome, the slice thickness measurement was 14.5 ± 3.4 μm (up to ~50% relative error); a nominal 24-μm section gave 24 ± 2.8 μm (up to ~10% relative error). It appears that the thickness of the microtome slices are accurate to a few micrometers, but this small error could result in sizable relative errors for thin slices.

B. Photobleaching Model Verification

Equation (10), which predicts photobleaching behavior as a function of both fluence and tissue thickness, was fitted to the data that was collected from five tissue sections. The model fit was obtained by setting $\kappa = 0.572\ (\mathrm{mJ}/\mu\mathrm{m}^2)^{-1}$ and $\mu = 0.0169\ \mu\mathrm{m}^{-1}$, while varying the constants C_R and C_{res}, which are expected to change owing to tissue inhomogeneities and instrumentation artifacts. The calculated values of C_R and C_{res} were then used to normalize the data and to obtain a normalized Raman signal $\bar{S}$ such that

$$\bar{S}(\Phi) = \frac{S_T(\Phi) - S_{\mathrm{res}}}{C_R/\mu}. \tag{15}$$

In Fig. 5, the normalized Raman signal is plotted for the five tissue sections as a function of tissue thickness Z_0 (panel A) and fluence Φ (panel B). The normalized photobleaching model predictions of Eq. (15) (dashed lines) are overlaid on the data (symbols). If one takes into account potential errors in tissue thickness and inhomogeneities in tissue composition, the model described by Eqs. (10) and (15) agrees well with the experimental data.

C. Excitation Power Effects

The model predicts that the power of the excitation light (the rate of energy delivery) only matters in that a given fluence will be reached faster with a more powerful beam. Thus Eq. (2) was linear in intensity I, and κ was taken to be constant. For verification purposes, photobleaching measurements were taken at three different excitation power levels from different locations on a 100-μm-thick tissue section. The results are plotted in Fig. 6. Although the residual Raman signal varies with power level, the initial slope, which is indicative of the photobleaching rate κ remains the same as the power is increased by a factor of 3 (from 0.275 to 0.8 mW). However, when the power is increased by a full order of magnitude (up to 2.15 mW), the initial slope becomes steeper, suggesting a higher value of κ, possibly due to nonlinear photobleaching effects at very high power levels. Also, at high power levels, no residual Raman signal was observed.

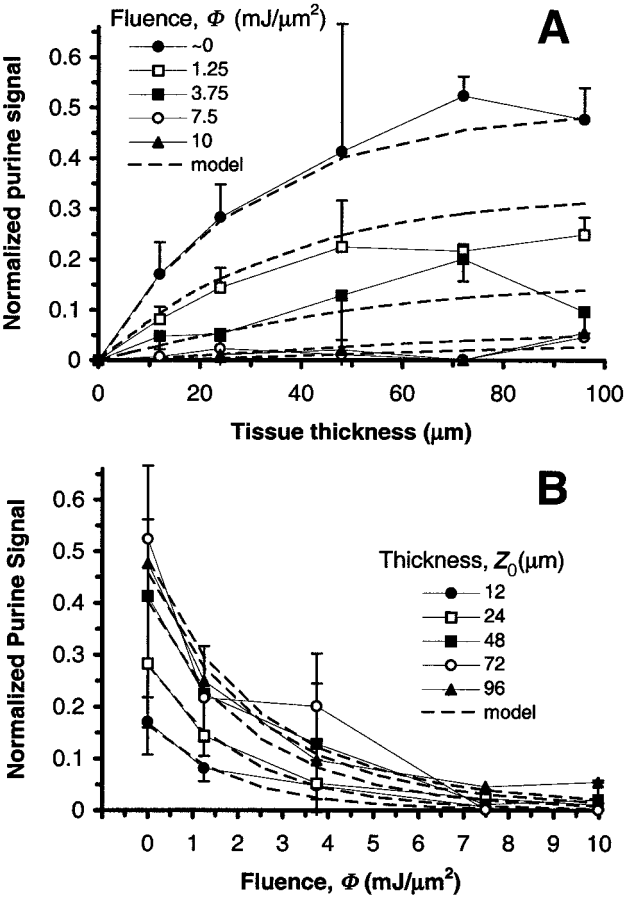

Fig. 5. Normalized purine signal as a function of thickness (A) and fluence (B) for five different tissue sections. Purine signal measurements were normalized according to Eq. (15). The normalized signal predicted from Eq. (15) (dashed curves) is overlaid on the measured data (symbols). The error bars represent the ±95% confidence interval of the mean. Error bars are plotted in one direction for clarity. When only one measurement was acquired, no error bar is shown.

5. Discussion

A model that predicts photobleaching as a function of fluence and tissue thickness was developed for human colon mucosa. This three-state model (Fig. 1) was preferred over one that describes individual photochemical reactions, since these reactions are very dependent on the local environment of the molecules and the molecules interaction with other species. A detailed description of the photochemistry of individual molecules would have been extremely difficult, since one would have had to keep track of all the different reactions and reaction rates that occur in a complex biologic system, such as colon mucosa. The purine photobleaching probability per unit fluence, $\kappa = 0.572 \pm 0.168\ (\mathrm{mJ}/\mu\mathrm{m}^2)^{-1}$, was quantified through measurement of the decrease in purine signal. The strength of an unbleached purine Raman band as a function of tissue thickness was used to calculate the attenuation coefficient $\mu = 0.0169 \pm 0.0023\ \mu\mathrm{m}^{-1}$. This value was in very good agreement with that obtained through absorption spectrophotometry ($\mu = 0.0160 \pm 0.0025\ \mu\mathrm{m}^{-1}$). With these measured values of μ and κ, the photobleaching model described by Eqs. (10) and (15) produced good fits to the measured data.

No other studies of absorption and photobleaching of colon mucosa at 250 nm were found in the litera-

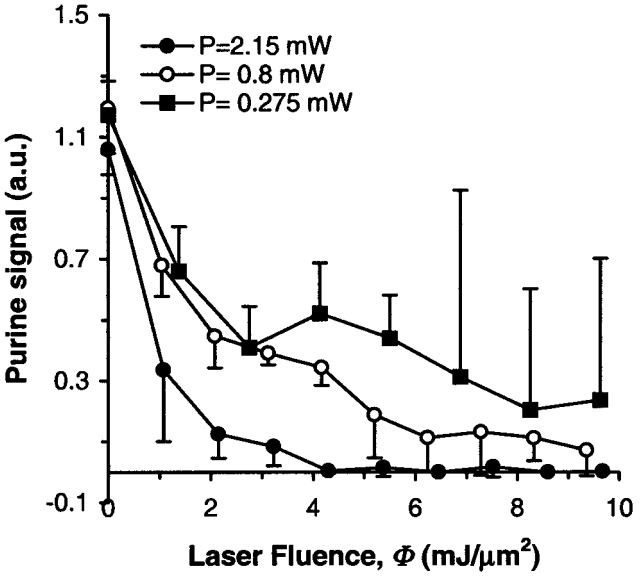

Fig. 6. Photobleaching rate as a function of laser power. Plots of purine signal versus laser fluence are shown for three different excitation power levels: 2.15 (filled circles), 0.8 (open circles), and 0.275 mW (filled squares). Data were collected from different locations on a 100-μm-thick colon section. Error bars represent the 95% confidence interval of the mean.

ture. Since absorption and photobleaching are strongly dependent on the sample composition and the excitation wavelength, a comparison of this study with those performed in aqueous solutions, with other tissues (not colon), or at different excitation wavelengths may not be completely adequate. Nonetheless, several measurements of attenuation coefficients at 250 nm for tissues other than colon are mentioned here for comparison. The attenuation coefficient of cornea was found to be 0.021 μm^{-1} at 248 nm,[15] that of cartilage at 250 nm was 0.055 μm^{-1},[16] that of epidermis was 0.1 μm^{-1} at 250 nm,[17] and that of stratum corneum was ~0.2 μm^{-1} at 250 nm.[18] The value of $\mu = 0.017 \pm 0.003$ μm^{-1} found in this study is on the lowest side of these values. The differences in the values that were measured for the different tissues are likely due to the differences in sample composition. Samples with a large cellular content would be expected to yield a large attenuation coefficient of approximately 250 nm, owing to the presence of nuclear material, which absorbs strongly at this wavelength. However, proteins may also contribute significantly to absorption at 250 nm. In particular, absorption by a given protein, such as collagen, in an impure form could be increased from its absorption in a pure state[19] and yield higher attenuation than is expected.

Several methods are available to determine the attenuation coefficient of tissue, defined as the sum of absorption (μ_a), and reduced scattering coefficient (μ_s').[20] Transmittance and reflectance measurements with an integrating sphere[21–24] and measurements of optical density with conventional instrumentation[15,16,18] are widely used. Other methods, such as measuring the complex index of refraction at a tissue-quartz interface for varying angles of incidence[14] or using backscattered power curves,[25] have also been proposed. In this study the effects of elastic scattering on the attenuation coefficient were assumed to be negligible compared with those of absorption at 251 nm. Thus two techniques were used to measure the attenuation coefficient: the first, by collecting Raman signals in a reflective-collection geometry; the second, by optical density measurement. Both methods gave similar values of μ and gave results that agreed with a model in which the effects of light scattering are negligible (Fig. 4). In the present measurements of μ, errors in the estimations of sample thickness are the likeliest source that accounts for the error bars in the presented data. The difficulty in reliably assessing the thickness of colon mucosa was noted previously.[22]

In the photobleaching study, one source of error in the measurement of κ was sample inhomogeneities, since data was averaged over different locations on a given specimen. However, in addition to this, several assumptions were made in the formulation of the model:

1. We assumed that $1/\mu \ll 80$ μm, the Rayleigh range of the excitation/collection lens. Thus the model was based on the collimated-beam geometry depicted in Fig. 2, and $K(z) = K_0$ in Eq. (6). We found $1/\mu = 60$ μm. While this is shorter than 80 μm, a longer focal-length objective could be used to lengthen the range of applicability of the model.
2. We assumed that the number of absorbers n_a in the tissue remains constant. As a result, Eqs. (2) and (3) were uncoupled, and light intensity was only a function of distance into the tissue. The plots of signal as a function of tissue thickness and fluence (Fig. 5) support this assumption. A fitting of the model to the data in the case of the coupled equations ($n_a = n_r$) resulted in significantly larger residuals than those obtained in the uncoupled case (data not shown). Thus the assumption that n_a is approximately constant is supported by the experimental data, which agree with the uncoupled equations presented in the text.
3. We assumed that the data collected within 100-s intervals corresponds to an instantaneous value of Raman signal (see Subsection 3.B), or that the fluence $\Phi(100\ s) \ll 1/\kappa$. We found $1/\kappa = 1.75$ $mJ/\mu m^2$. With $I_0 \sim 0.01$ $mW/\mu m^2$, a fluence of 1 $mJ/\mu m^2$ is reached in 100 s. Although this value of fluence is less than $1/\kappa$, an exposure time of less than 100 s would have better approximated an instantaneous measurement. To estimate the error in signal that is due to the signal decrease during the 100-s acquisition period, we could integrate the Raman signal over the collection interval $\Delta t = 100$ s and compare the results with the case where $\kappa = 0$ (no photobleaching). The largest error will occur where the decrease in signal is largest, i.e., near $\Phi \sim 0$ (initial slope), and for the thinnest section. For a thin section, the relative decrease in S_R that is due to

photobleaching is the ratio of the integral of S_R in relation (13) to the integral the signal in the absence of photobleaching,

$$100\left[1 - \frac{1 - \exp(-\kappa\Phi)}{\kappa\Phi_0}\right]. \quad (16)$$

Thus, for $\Phi_0 = 1$ mJ/μm^2 (first 100-s time interval), the signal measured is at most 23.85% less than that assumed by the model (not accounting for S_{res}). However, this error does not affect our calculation of κ, obtained by fitting relation (13) to the data for the 12-μm section. If instead of relation (13) we consider the integral of S_T over each 100-s interval as a function of Φ, we find that

$$\int_{\Delta t=100s} S_T(\Phi)|_{Z_0\to 0} \approx \frac{C_R Z_0}{\kappa}[1 - \exp(-\kappa I_0 \Delta t)] \times \exp(-\kappa\Phi) + C_{\text{res}} z_0. \quad (17)$$

In the nonlinear data-fitting routine an equation of the form $A[\exp(-\kappa\Phi)]+B$ was used, where A, κ, and B were varied. Relation (17) is still of the same form, although instead of $A = C_R Z_0$ as in relation (13), now $A = (C_R Z_0/\kappa)[1 - \exp(-\kappa I_0 \Delta t)]$. Thus the resulting κ remains unchanged. Still, the 24% error in $S_T(\Phi \sim 0)$ for thin slices may account for a 24% underestimate of μ. In the absence of photobleaching, the initial slope would have been steeper in Fig. 4A. From relation (16) we can also deduce that a fluence under 0.2 mJ/μm^2 must be used to collect spectra that have less than 5% purine photobleaching for thin sections.

Finally, although the model assumed no dependence of photobleaching rate on laser power [Eq. (2) was linear in intensity I], the results showed that this was not the case when the power was increased by one order of magnitude (Fig. 6). This may be due to nonlinear transitions that involve more than one photon. Nonlinear transitions have been described previously for powerful UV irradiation of DNA bases.[26,27] On the other hand, the dependence of κ on laser power may also be due to tissue heating. Temperature rise at the irradiated spot will depend on laser power and could increase the photobleaching rate. Notably in our studies (not shown here), photobleaching was found to be greatly increased when the spectra were collected at room temperature.[28]

6. Implications of the Study

The measured penetration depth D, taken as $1/\mu$, was approximately 60 μm. However, the UVRR spectra are typically collected in a backscattered geometry. Thus the tissue sampling depth is actually $1/2\ \mu = 30\ \mu$m, since the light travels into the tissue and back to the sample surface as the Raman signal is collected. For colon mucosa, this implies that ~65% of the Raman signal is collected from the epithelium, and the remaining ~35% is collected from the underlying tissue (lamina propria).

The photobleaching rate determined by this study was found to be $\kappa = 0.572$ (mJ/μm^2)$^{-1}$. This implies that fluences well under 1.75 mJ/μm^2 ($1/\kappa$) are necessary in the collection of unbleached purine signals in thin tissue sections. For example, a fluence of less than 0.2 mJ/μm^2 is necessary in the collection of spectra with less than 5% purine photobleaching from a thin colon section. Signal decrease that is due to photobleaching will be slower as the sample thickness is increased. Finally, the photobleaching rate κ remained independent of power P for $P < 1$ mW. However, higher power values resulted in higher photobleaching rates, potentially due to nonlinear effects.

I thank Ramachandra Dasari, James Crawford, and Michael Feld for their support and guidance. J. Crawford's help was also essential in the collection and preparation of the colon specimens used in this study. I also thank L. Perelman, I. Itzkan, J. Brennan, and R. Manoharan for useful discussions. Research was conducted at the Massachusetts Institute of Technology Biomedical Research Center supported by NIH-P41-RR02594. Additional support was provided by NIH RO1-CA53717 and NSF-9304251.

References

1. F. Sureau, L. Chinsky, C. Amirand, J. P. Ballini, M. Dusquesne, A. Laigle, P. Y. Turpin, and P. Vigny, "An ultraviolet micro-Raman spectrometer: resonance Raman spectroscopy within single cells," Appl. Spectrosc. **44,** 1047–1051 (1990).
2. W. H. Nelson, R. Manoharan, and J. F. Sperry, "UV resonance Raman studies of bacteria," Appl. Spectrosc. Rev. **27,** 67–124 (1992).
3. S. Chadha and W. H. Nelson, "Ultraviolet micro-Raman spectrograph for the detection of small numbers of bacterial cells," Rev. Sci. Instrum. **64,** 3088–3093 (1993).
4. R. Manoharan, Y. Wang, R. Dasari, S. S. Singer, R. P. Rava, and M. S. Feld, "Ultraviolet resonance Raman spectroscopy for detection of colon cancer," Lasers Life Sci. **6,** 1–11 (1994).
5. V. Pajcini, C. H. Munro, R. W. Bormett, R. E. Witkowski, and S. A. Asher, "UV Raman microspectroscopy: spectral and spatial selectivity with sensitivity and simplicity," Appl. Spectrosc. **51,** 81–86 (1997).
6. Y. Yazdi, N. Ramanujam, R. Lotan, M. M. Follen, W. Hittelman, and R. Richards-Kortum, "Resonance Raman spectroscopy at 257 nm excitation of normal and malignant cultured breast and cervical cells," Appl. Spectrosc. **53,** 82–85 (1999).
7. N. N. Boustany, J. M. Crawford, R. Manoharan, R. R. Dasari, and M.S. Feld, "Analysis of nucleotides and aromatic amino acids in normal and neoplastic colon mucosa with ultraviolet resonance Raman spectroscopy," Lab. Invest. **79,** 1201–1214 (1999).
8. N. N. Boustany, R. Manoharan, R. R. Dasari, and M. S. Feld, "Ultraviolet Raman spectroscopy of bulk and microscopic colon tissue," Appl. Spectrosc. **54,** 24–30 (2000).
9. M. H. Patrick and R. O. Rahn, "Photochemistry of DNA and polynucleotides: photoproducts," in *Photochemistry and Photobiology of Nucleic Acids*, S. Y. Wang, ed. (Academic, New York, 1976),Vol. 2.
10. D. Strommen and K. Nakamoto, *Laboratory Raman Spectroscopy* (Wiley, New York, 1984), pp. 115, 118.
11. G. Dellepiane and J. Overend, "Vibrational spectra and assignment of acetone, $\alpha\alpha\alpha$ acetone-d_3 and acetone-d_6," Spectrochim. Acta **22,** 593–614 (1966).
12. S. T. Wollman and P. W. Bohn, "Evaluation of polynomial fitting functions for use with CCD arrays in Raman spectroscopy," Appl. Spectrosc. **47,** 125–126 (1993).

13. W. H. Press, S. A. Teulosky, W. T. Vetterling, and B. P. Flannery, *Numerical Recipes in C: the Art of Scientific Computing*, 2nd ed. (Cambridge U. Press, New York, 1992).
14. G. H. Pettit and M. N. Ediger, "Corneal-tissue absorption coefficients for 193- and 213-nm ultraviolet radiation," Appl. Opt. **35,** 3386–3391 (1996).
15. C. A. Puliafito, R. F. Steinert, T. F. Deutsch, F. Hillenkamp, E. J. Dehm, and C. M. Adler, "Excimer laser ablation of the cornea and lens: experimental studies," Ophthalmology **92,** 741–748 (1985).
16. J. Raunest and H-J. Schwarzmaier , "Optical properties of human articular tissue as implication for a selective laser application in arthroscopic surgery," Lasers Surg. Med. **16,** 253–261 (1995).
17. V. V. Tuchin, S. R. Utz , and I. V. Yarolavsky, "Tissue optics, light distribution, and spectroscopy," Opt. Eng. **33,** 3178–3188 (1994).
18. M. A. Everett, E. Yeargers, R. M. Sayre, and R. L. Olson, "Penetration of epidermis by ultraviolet rays," Photochem. Photobiol. **5,** 533–542 (1966).
19. J. R. Loofbourow, B. S. Gould, and I. W. Sizer, "Studies on the ultraviolet absorption spectra of collagen," Arch. Biochem. **22,** 406–411 (1949).
20. B. C. Wilson and S. L. Jacques, "Optical reflectance and transmittance of tissues: principles and applications," IEEE J. Quantum Electron. **26,** 2186–2199 (1990).
21. E. Chan, T. Menovsky, and A. J. Welch, "Effect of cryogenic grinding on soft-tissue optical properties," Appl. Opt. **35,** 4526–4532 (1996).
22. R. Marchesini, E. Pignoli, S. Tomatis, S. Fumagalli, A. E. Sichirollo, S. Di Palma, M. Dal Fante, P. Spinelli A. C. Croce, and G. Bottiroli, "*Ex vivo* optical properties of human colon tissue," Lasers Surg. Med. **15,** 351–357 (1994).
23. G. L. Zonios, R. M. Cothren, J. T. Arendt, J. Wu, J. Van Dam, J. M. Crawford, R. Manoharan, and M. S. Feld, "Morphological model of human colon tissue fluorescence," IEEE Trans. Biomed. Eng. **43,** 113–122(1995).
24. W. F. Cheong, S. A. Prahl, and A. J. Welch, "A review of the optical properties of biological tissues," IEEE J. Quantum Electron. **26,** 2166–2185 (1990).
25. J. M. Schmitt, A. Knuttel, and R. F. Bonner, "Measurement of optical properties of biological tissues by low-coherence reflectometry," Appl. Opt. **32,** 6032–6042 (1993).
26. G. G. Gurzadyan, R. K. Ispiryan, and K. Sh. Voskanyan, "Two-quantum photoprocesses in DNA under picosecond laser UV irradiation at 216 and 270 nm," J. Photochem. Photobiol. B **11,** 269–275 (1991).
27. D. N. Nikogosyan, D. A. Angelov, and A. A. Oraevsky, "Determination of parameters of excited states of DNA and RNA bases by laser UV photolysis," Photochem. Photobiol. **35,** 627–635 (1982).
28. N. N. Boustany, J. M. Crawford, R. Manoharan, R. R. Dasari, and M. S. Feld, "Effects of freeze-thaw and photobleaching on the ultraviolet Raman spectra of human colon biopsies," Appl. Spectrosc. (to be published).
29. J. R. Taylor, *An Introduction to Error Analysis: the Study of Uncertainties in Physical Measurements* (University Science Books, Mill Valley, Calif., 1982).